Int. J. Heat Mass Transfer. Vol. 23, pp. 471–481
© Pergamon Press Ltd. 1980. Printed in Great Britain.

0017–9310/80/0401–0471 $02.00/0

HEAT TRANSFER AND FLUID FLOW CHARACTERISTICS OF SPANWISE-PERIODIC CORRUGATED DUCTS

E. M. SPARROW and M. CHARMCHI

Department of Mechanical Engineering, University of Minnesota, Minneapolis, MN 55455, U.S.A.

(*Received* 1 *August* 1979 *and in revised form* 25 *September* 1979)

Abstract – An analytical study is made of the laminar flow and heat transfer in ducts whose cross section is bounded by a wall with periodic corrugations distributed across the span; the other bounding wall is parallel to the corrugated wall and is plane. The study consists of two parts, the first of which is aimed at providing basic heat transfer and fluid flow results while the second utilizes and illuminates these results by means of performance evaluations and comparisons. The basic results, determined numerically, encompass Nusselt numbers, friction factors, isovels and isotherms, and cross sectional mass flow distributions. For the performance evaluations, comparisons were made between the corrugated-wall duct and the parallel plate channel. It was demonstrated that if the temperature of the duct wall is to be minimized, as in an air-operated solar collector, a corrugated duct can be highly effective, but at the price of additional surface area and greater duct height.

NOMENCLATURE

A, cross sectional area;
A_Δ, cross sectional area of triangle bounded by corrugations;
c, height of clearance gap, Fig. 1;
c_p, specific heat;
D_e, equivalent diameter, equation (2);
f, friction factor, equation (13);
H, height of parallel plate channel;
h, height of corrugations, Fig. 1;
k, thermal conductivity;
$\dot{m}$, mass flow rate;
$\dot{m}_\Delta$, flow rate through area A_Δ;
Nu, Nusselt number, equation (16);
P, pumping power, $(\dot{m}/\rho)\Delta p$;
p, pressure;
Q', heat-transfer rate per unit axial length;
$\bar{q}$, average flux at heated surface;
Re, Reynolds number, $\bar{u}D_e/\nu$;
S, surface area of heated wall;
T, temperature;
T_b, bulk temperature;
T_{cw}, temperature of corrugated wall;
T_w, wall temperature;
U, dimensionless velocity, equation (1);
$\bar{U}$, mean value of U, equation (8),
u, axial velocity;
$\bar{u}$, mean axial velocity;
X, dimensionless coordinate, x/D_e;
Y, dimensionless coordinate, y/D_e;
x, spanwise coordinate;
y, normal coordinate;
z, axial coordinate.

Greek symbols

α, corrugation angle, Fig. 1;
θ, dimensionless temperature, $(T - T_{cw})/(Q'/k)$;
θ_b, bulk value of θ;
μ, viscosity;
ν kinematic viscosity;
ρ, density.

Subscript

0, parallel plate channel.

INTRODUCTION

THERE is a rich variety of duct cross sectional shapes that are of heat transfer interest, as witnessed by the Shah–London monograph [1] where the world literature on laminar duct-flow heat transfer has been brought together. That monograph not only displays the abundance of information available for various cross sections but also provides, by omission, perspectives on important classes of flow configurations whose characteristics remain unexplored or are only partially explored. One such class encompasses ducts whose flow cross section possesses spanwise periodicity. An example of such a duct is pictured in cross sectional view in Fig. 1, with the direction of fluid flow being perpendicular to the plane of the figure. As seen in the figure, the upper boundary of the duct is a spanwise-periodic corrugated wall while the lower wall is plane. These walls thus define a flow cross section which is spanwise periodic.

The spanwise-periodic corrugated duct shown in Fig. 1 is the focus of the present research. The research consists of two interrelated parts. In the first, basic heat transfer and fluid flow information, encompassing the Nusselt number, friction factor, mass flow distribution, and velocity and temperature fields, is obtained from numerical solutions for a range of values of the corrugation angle and the dimension ratio c/h (see Fig.

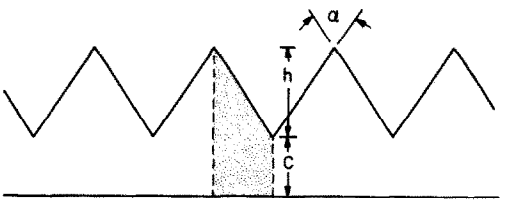

FIG. 1. Spanwise-periodic corrugated duct.

1 for nomenclature). Then, in the second part, this basic information is employed to compare the performance of spanwise-periodic corrugated ducts of various corrugation angles and dimension ratios with that of other ducts which might serve as alternatives for the same application. These comparisons are made for practice-oriented scenarios where performance objectives and constraints are specified.

The concern of the present paper with performance evaluation is somewhat unusual in that the overwhelming majority of research publications on duct-flow heat transfer (e.g. those cited in [1]) do not go beyond the reporting of the basic results. The present concern with performance stems from the realization that the spanwise-periodic corrugated duct can be regarded as an enhanced geometry and it is, therefore, logical to examine the degree of enhancement that can be attained.

That the corrugations provide the possibility of enhancement can be recognized by envisioning the corrugated wall of Fig. 1 replaced by a plane surface that is parallel to the lower wall. By comparing the surface area that would be washed by fluid passing through the corrugated-wall duct and the parallel plate channel, it is evident that the corrugations increase the surface area. The area increase serves to increase the capacity of the surface to transfer heat or, alternatively, enables the transfer of a given amount of heat at a lower wall-to-bulk temperature difference. There are, of course, fluid flow considerations that have to be dealt with, and these will be taken into account in the quantitative performance evaluations to be described later.

In connection with the aforementioned surface area enhancement, it is relevant to observe that the authors' first exposure to the spanwise-periodic corrugated duct was via an air-operated solar collector application where such enhancement was being sought [2]. In the design of flat-plate solar collectors with air as the transfer fluid, cognizance has to be taken of the fact that the fluid-to-surface heat-transfer coefficients are much smaller than those in water-operated collectors. Therefore, to transfer the same amount of heat at a comparable temperature difference between the fluid and the collector plate, the transfer surface area in an air-operated collector has to be much greater than that in a water-operated collector.

Typically, in present-day air-operated flat-plate collectors, the flow passage is a parallel plate channel bounded above by the collector plate and below by an insulated wall. Based on available information [3], a channel Reynolds number of 2300 was calculated as corresponding to one of the standard operating modes. This suggests laminar flow, especially since it was demonstrated in [4] that transition to turbulence in a parallel plate channel occurs at Reynolds numbers of 2600 or greater if the sources of disturbance are not situated within the channel proper.

Although some consideration will be given to the aforementioned solar collector application, all of the basic results to be presented here are completely general. The performance evaluations will make use of the collector application as a focal point, but the conclusions drawn from the performance comparisons can be given broader significance.

From an examination of Fig. 1, it is seen that certain symmetries prevail so that the solution domain can be restricted to the speckled region. This region does not fit conveniently into any standard coordinate system. Even if the inclined boundary is approximated in a staircase fashion, the resulting solution domain is unacceptable to most general-purpose finite difference computer codes, which are structured to work with domains that are rectangles. To deal with this situation, use will be made of a technique recently suggested by Patankar [5] which will enable the solution domain to be transformed into a rectangle.

Solutions will be obtained for fully developed laminar flow and heat transfer. The thermally developed state to be treated here is the result of a heat input at the corrugated wall which is uniform per unit of length in the axial direction. In any cross section, the temperature of the corrugated wall is spanwise uniform. The lower wall of the duct is adiabatic. The solutions, obtained via numerical finite differences, depend on two parameters – the corrugation angle α and the dimension ratio c/h. Values of α were assigned as 20, 40, 60, and 90°. For each angle, c/h was varied systematically between zero and one. Typically, about ten c/h values were required to accurately define the variation of the Nusselt number and friction factor over this range.

A search of the literature did not reveal any prior results for the spanwise-periodic corrugated duct. With regard to spanwise-periodic ducts in general, a broad definition might encompass tubes with internal fins and tubes with circumferentially periodic surface waviness – cited in [1]. Also available in [1] are results for the parallel plate channel and for isosceles triangular ducts that will be employed in subsequent sections of the paper.

ANALYSIS

To facilitate the problem formulation, the typical module which constitutes the solution domain is shown in Fig. 2 along with the coordinates and other nomenclature. At this juncture, the solution domain is defined by the region ABCEA, but it will be modified during the course of the analysis.

The governing equations for the velocity and temperature problems encompass the conservation laws for mass, momentum, and energy. For constant-property, incompressible flow, the velocity problem can be solved without reference to the temperature. To obtain a dimensionless representation of the velocity field equations, new variables are introduced as follows

$$X = x/D_e, \quad Y = y/D_e, \quad U = u/[(-\mathrm{d}p/\mathrm{d}z)D_e^2/\mu] \quad (1)$$

where x and y are the cross sectional coordinates as

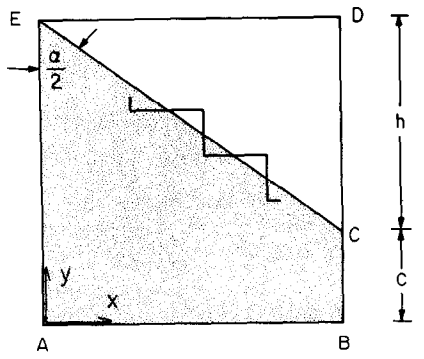

FIG. 2. Typical module of duct cross section.

depicted in Fig. 2, and z is the axial coordinate. The equivalent diameter D_e appearing in equation (1) is given by

$$D_e = 4h(c/h + \tfrac{1}{2})/[1 + \text{cosec}(\alpha/2)]. \quad (2)$$

Consistent with fully developed flow, the axial pressure gradient $\mathrm{d}p/\mathrm{d}z$ is a constant, the transverse velocity $v = 0$, and the inertia terms vanish identically. For these conditions, the mass conservation equation reduces to $\partial U/\partial z = 0$ and momentum conservation becomes

$$\partial^2 U/\partial X^2 + \partial^2 U/\partial Y^2 + 1 = 0. \quad (3)$$

For the formulation of the energy equation, note is taken of the uniform heating Q' per unit axial length at the inclined surface CE and of the adiabatic condition at the lower wall AB and on the symmetry lines BC and AE. Since $\partial T/\partial z = \partial T_b/\partial z$ in a thermally developed uniformly heated flow, then

$$\partial T/\partial z = Q'/\dot{m}c_p. \quad (4)$$

As indicated earlier, the temperature at the corrugated wall is assumed to be spanwise uniform, but there is a linear variation in the axial direction in accordance with equation (4). At a representative axial station in the thermally developed regime, the temperature of the corrugated wall may be denoted by T_{cw} and, with this, a dimensionless temperature θ is defined as

$$\theta = (T - T_{cw})/(Q'/k). \quad (5)$$

Since both T and T_{cw} vary linearly with z in the same manner, the quantity $(T - T_{cw})$ is independent of z, as is θ. However, both T and θ vary with x and y.

With the foregoing inputs, the energy equation takes the form

$$(U/\bar{U})F(\alpha, c/h) = \partial^2\theta/\partial X^2 + \partial^2\theta/\partial Y^2 \quad (6)$$

in which

$$F(\alpha, c/h) = 16(c/h + \tfrac{1}{2})/ [1 + \text{cosec}(\alpha/2)]^2 \tan(\alpha/2) \quad (7)$$

and $\bar{U}$ is the dimensionless mean velocity defined as

$$\bar{U} = \int U \,\mathrm{d}A / \int \mathrm{d}A \quad (8)$$

where the integrals are evaluated over the flow cross section.

The governing equations (3) and (6) for the velocity and temperature fields are supplemented by the following boundary conditions

$$\text{On AB: } U = 0 \text{ and } \partial\theta/\partial Y = 0 \quad (9a)$$

$$\text{On BC: } \partial U/\partial X = \partial\theta/\partial X = 0 \quad (9b)$$

$$\text{On CE: } U = 0 \text{ and } \theta = 0 \quad (9c)$$

$$\text{On EA: } \partial U/\partial X = \partial\theta/\partial X = 0. \quad (9d)$$

The coordinates of the aforementioned boundaries involve both α and c/h, and these quantities also appear directly in equation (6). Therefore, the solutions depend parametrically on assigned values of α and c/h.

In view of the shape of the solution domain ABCEA, it is clear that an analytical solution is out of range. A finite difference approach can be used to yield results of high accuracy by approximating the inclined boundary CE in a staircase manner as indicated by the representative segment shown in Fig. 2. Although such an approximation provides a solution domain whose boundaries coincide with coordinate lines in a Cartesian system, the domain is not a rectangle. This characteristic does not fit very well with the capabilities of many general-purpose computer codes which are structured to deal with domains which are rectangles.

By employing a technique recently devised by Patankar [5], the solution domain can be transformed into a rectangle, thereby enabling solutions to be obtained by application of general-purpose finite difference codes. The solution domain to be used here is the rectangle ABCDEA, on whose boundaries the following conditions are assigned

$$\text{On AB: } U = 0 \text{ and } \partial\theta/\partial Y = 0 \quad (10a)$$

$$\text{On BC: } \partial U/\partial X = \partial\theta/\partial X = 0 \quad (10b)$$

$$\text{On CD and DE: } U = 0 \text{ and } \theta = 0 \quad (10c)$$

$$\text{On EA: } \partial U/\partial X = \partial\theta/\partial X = 0. \quad (10d)$$

The rectangular region is envisioned as being filled with a fluid having the following properties

$$\text{In ABCEA: } \mu \text{ and } k \text{ have values equal to those of the actual fluid} \quad (11a)$$

$$\text{In CDEC: } \mu = \infty \text{ and } k = \infty \quad (11b)$$

where it is now understood that there is a staircase line connecting points C and E.

The specification of $\mu = \infty$ (11b), coupled with boundary condition (10c), suppresses all motion in region CDEC and makes $U = 0$ on the line CE. Similarly, the use of $k = \infty$ in CDEC causes θ to be zero along CE. It is important to note that CE is an internal line in the transformed domain and no conditions are actually imposed along it.

The transformed problem is characterized by a fluid having stepwise discontinuities of viscosity and thermal conductivity, and provision has to be made in the finite difference representation to accommodate such changes. In [5], on the basis of limiting cases and numerical examples, Patankar recommended that the harmonic mean viscosity and thermal conductivity be used. Thus, for example, at the interface between two control volumes having viscosities μ_i and μ_{i+1} respectively, the harmonic mean viscosity is given by

$$\mu = 2\mu_i\mu_{i+1}/(\mu_i + \mu_{i+1}) \tag{12}$$

and similarly for the thermal conductivity. This expression was used to evaluate the viscosity (and thermal conductivity) at all control volume faces, but its special attributes were activated only at discontinuity surfaces.

The finite difference scheme employed here has been accorded book-length description in a forthcoming text [6], and no elaboration is necessary here aside from that of the foregoing paragraphs. With regard to the finite difference grid, 25×48 points, respectively for the x- and y-directions, were used for the case of $c/h = 0$ (i.e. for the triangular duct). With increasing values of c/h, the points were redeployed into a 20×70 distribution. The solutions were iterative but convergence was rapid owing to a block iteration procedure. The results of certain accuracy tests will be discussed shortly.

FLUID FLOW AND HEAT-TRANSFER RESULTS

The two quantities that are of most direct applicability are the friction factor and the Nusselt number. Results for these quantities are presented in this section of the paper, as are velocity and temperature contour diagrams and distributions of mass flow.

Friction factor and Nusselt number

The friction factor is evaluated from its customary definition

$$f = (-\mathrm{d}p/\mathrm{d}z)D_e/\tfrac{1}{2}\rho\bar{u}^2 \tag{13}$$

which becomes, in terms of the variables of the analysis

$$fRe = 2/\bar{U} \tag{14}$$

where the dimensionless mean velocity $\bar{U}$ is from equation (8) and

$$Re = \bar{u}D_e/\nu. \tag{15}$$

An average heat-transfer coefficient for the corrugated wall may be defined by noting that the rate of heat transfer per unit surface is $Q'/h\sec(\alpha/2) \equiv \bar{q}$. The average Nusselt number then follows as

$$Nu = [\bar{q}/(T_{cw} - T_b)]D_e/k \tag{16}$$

or

$$Nu = -[(D_e/h)\cos(\alpha/2)]/\theta_b \tag{16a}$$

where D_e/h is expressed by equation (2) and the dimensionless bulk temperature θ_b is computed from

$$\theta_b = \int \theta U \,\mathrm{d}A / \int U \,\mathrm{d}A. \tag{17}$$

The fRe product evaluated from equation (14) is plotted in Fig. 3 as a function of the dimension ratio c/h, with the corrugation angle α as curve parameter. From the figure, it can be seen that an increase in the clearance gap between the corrugated and plane walls has a somewhat different effect on fRe depending on the corrugation angle. For $\alpha = 90°$, the fRe curve increases monotonically with c/h, although at a lesser rate at larger c/h. On the other hand, the curve for $\alpha = 20°$ decreases monotonically and substantially after attaining an initial maximum. The results for the other cases display an intermediate behavior.

In appraising the impact of these trends on the pressure drop, it is important to take note of the fact that the observed changes in fRe may be caused by various factors. Suppose, for instance, that the clearance c is increased for fixed values of h and α. For these

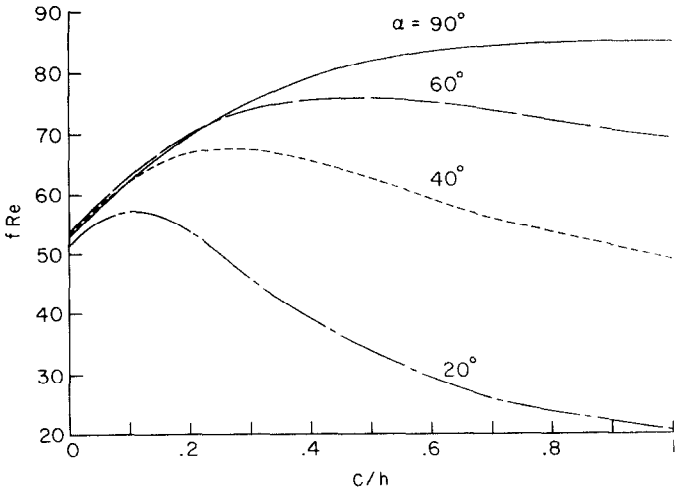

FIG. 3. Friction factor results.

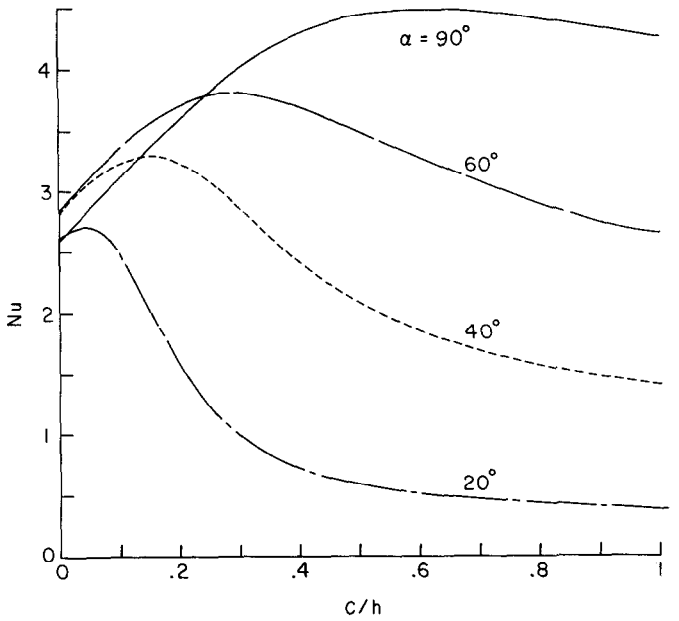

FIG. 4. Nusselt number results.

conditions, equation (2) shows that the equivalent diameter D_e increases with increasing c/h; this increase is much more rapid at large corrugation angles than at small corrugation angles. Since D_e appears linearly in the friction factor, its increase with c/h tends to promote the same behavior in fRe at a fixed Reynolds number.

From a replot of the friction factor results (not shown here), it was found that the pressure gradient group $(-dp/dz)/\frac{1}{2}\rho\bar{u}^2$ decreases with c/h for fixed values of h, α, and Re. With this information, the shapes of the curves of Fig. 3 can be rationalized in terms of opposing influences of D_e and $(-dp/dz)/\frac{1}{2}\rho\bar{u}^2$ with c/h. Clearly, the former wins out at higher α values, with the opposite outcome at the smaller α values.

Attention will now be turned to the Nusselt number results of Fig. 4. In this figure, Nu is plotted as a function of c/h for parametric values of α. From an examination of Figs. 3 and 4, it can be seen that the trends that were identified in the former are also in evidence in the latter. Furthermore, the competing ingredients which influence the friction factor results have their counterparts for the Nusselt number. In particular, for given values of h and α, the heat-transfer coefficient decreases with c/h while D_e increases. There is a greater downsloping tendency in evidence in Fig. 4 than in Fig. 3, suggesting that the heat-transfer coefficient decreases somewhat more rapidly with c/h than does $(-dp/dz)/\frac{1}{2}\rho\bar{u}^2$.

Whereas the pressure group and the heat-transfer coefficient respond in a qualitatively similar manner to changes in c/h and α, the impact of these responses on design decisions remains unclear. This matter will be revisited later in the paper, when performance evaluations are presented.

Before concluding the friction factor and Nusselt number presentation, mention may be made of certain comparisons with the literature. The only possible comparisons are for the case of $c/h = 0$ (isosceles triangular ducts). Analytical solutions for the 60° and 90° ducts, reported in [1], gave fRe values that differed by about 0.5% from the present numerical solutions. This level of agreement is satisfactory for any contemplated application. Higher accuracies are expected for cases where $c/h > 0$ since the portion of the solution domain between $y = 0$ and $y = c$ is truly rectangular. The available heat-transfer results for isosceles triangular ducts are based on finite difference solutions. Nusselt numbers obtained with the present computer program agreed with results tabulated in [1] in the range from 0 to 0.6%. Upon recognizing that both sets of compared solutions are necessarily inexact, this level of agreement is entirely satisfactory.

Isovels, isotherms, and mass flow distributions

Insights into the nature of the velocity and temperature fields and their response to α and c/h can be obtained by examining contour diagrams which show isovels and isotherms. The presentation of results will be made for two corrugation angles*, $\alpha = 90$ and 40°, and for each angle information will be presented for the smallest and largest of the investigated values of c/h, namely, zero and one.

Figures 5(a) and (b) display the isovels and isotherms for $\alpha = 90°$, respectively for $c/h = 0$ and 1. In each figure, the isovels appear at the left and the isotherms at the right. The plotted isovels are actually contours of $u/\bar{u}$ while the isotherms are contours of

* Initially, it was planned to use $\alpha = 90$ and 20°, but the narrowness of the 20° case prevented a clear portrayal of the results.

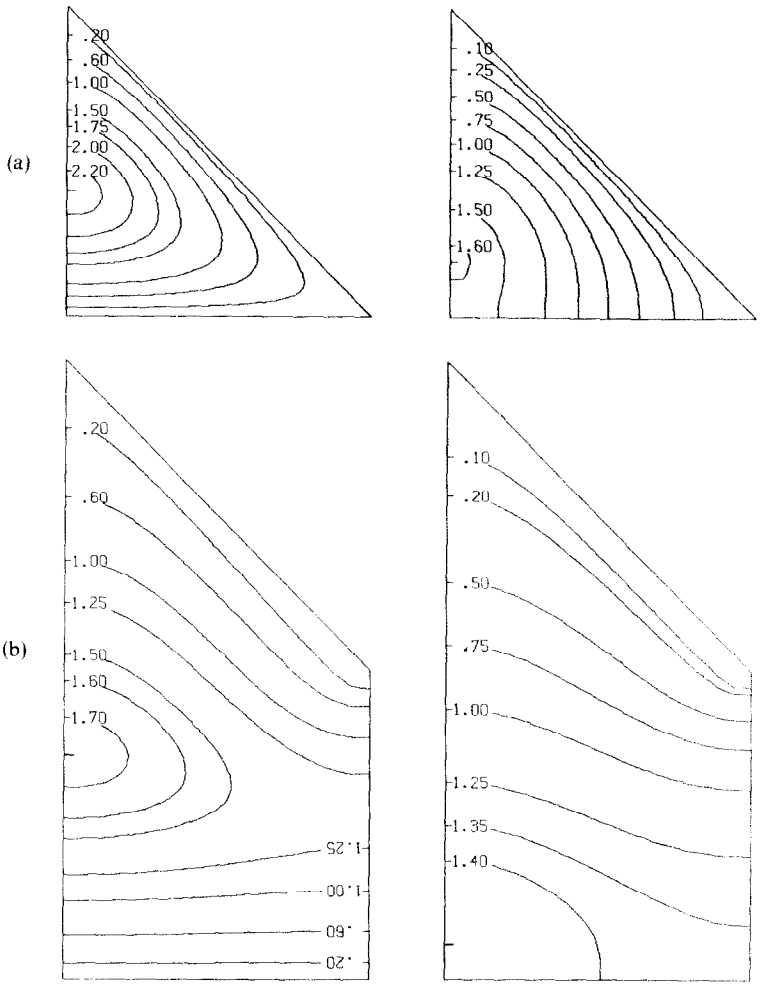

FIG. 5. (a) Isovels $u/\bar{u}$ (left) and isotherms θ/θ_b (right) for $\alpha = 90°$ and $c/h = 0$; $(u/\bar{u})_{max} = 2.26$ and $(\theta/\theta_b)_{max} = 1.61$. (b) Isovels and isotherms for $\alpha = 90°$ and $c/h = 1$; $(u/\bar{u})_{max} = 1.74$ and $(\theta/\theta_b)_{max} = 1.44$.

$(T - T_{cw})/(T_b - T_{cw}) = \theta/\theta_b$; the curve labels correspond to values of these quantities. The locations of the maximum values of $u/\bar{u}$ and θ/θ_b are indicated in the respective diagrams by a short tic, with the values themselves being stated in the figure captions.

In general, the isovels and isotherms are of a somewhat different character owing to the difference between the boundary conditions at the lower boundary ($y = 0$). The zero velocity condition at that boundary, in contrast to the zero derivative for the temperature, gives rise to variations of $u/\bar{u}$ that are more rapid than those of θ/θ_b. Furthermore, whereas the isovels are more or less parallel to the lower boundary, the isotherms are perpendicular to that boundary. In addition, $(u/\bar{u})_{max}$ is larger than $(\theta/\theta_b)_{max}$.

Comparison of Figs. 5(a) and (b) show that the presence of a substantial clearance (i.e. $c/h = 1$) causes numerous changes in the contour diagrams relative to the no-clearance case ($c/h = 0$). The variations of both the velocity and temperature are more gradual and the respective peak values are lower. Furthermore, the contour lines are no longer closed; rather they connect with mirror-image curves at the symmetry boundary. Of particular interest is the fact that the point of maximum velocity and the surrounding high-velocity contours are situated in the clearance space below the corrugations, suggesting that a relatively large fraction of the total mass flow passes through that region. This issue will be revisited shortly.

The contour diagrams for the $\alpha = 40°$ case are presented in Fig. 6 for both $c/h = 0$ and $c/h = 1$. As before, for each c/h, the velocity is at the left and the temperature is at the right. Except for their elongation, the 40° contours for $c/h = 0$ are similar to those for 90°. The 40° contours for $c/h = 1$ also exhibit general similarity with the 90° contours, but there are interesting differences in detail in the lower part of the flow passage. In particular, for the 40° case, both the isovels and isotherms are horizontal lines, indicating that in that region the velocity and temperature fields depend only on a single coordinate, namely, the distance from the wall. Thus, the fluid passing through the lower part of the flow passage appears to be unaware of the inclined upper boundary, which is not surprising in view of the narrowness of the module.

Attention is now turned to the distribution of the

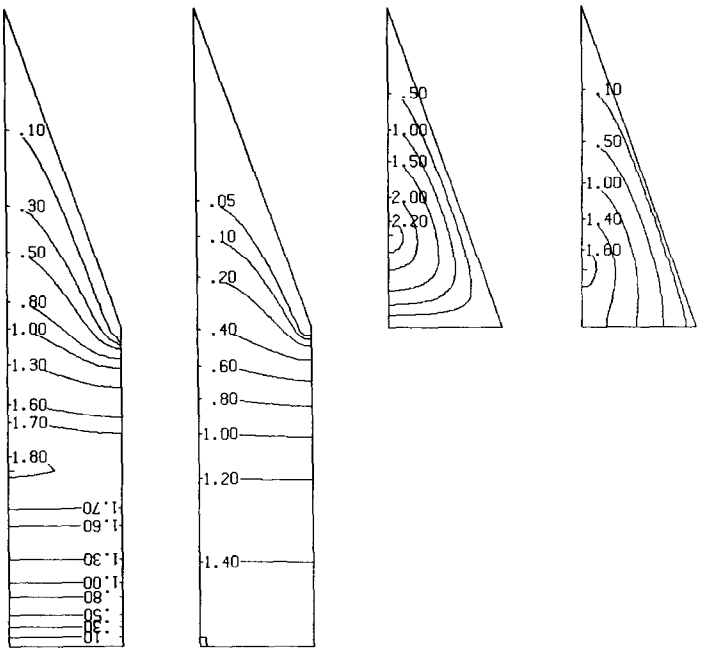

FIG. 6. Isovels and isotherms for $\alpha = 40°$ and $c/h = 0$ and 1; $(u/\bar{u})_{max} = 2.25$, 1.81 and $(\theta/\theta_b)_{max} = 1.63$, 1.43.

mass flow in the cross section. In this connection, let $\dot{m}_\Delta$ denote the mass flow in the triangular region defined by the corrugations and bounded below by $y = c$. Also, let the total mass flow in the cross section as a whole be denoted by $\dot{m}$. Thus, the ratio $\dot{m}_\Delta/\dot{m}$ gives the fraction of the mass flow which passes through the triangular region, and $1 - \dot{m}_\Delta/\dot{m}$ is the fraction passing through the clearance gap.

Figure 7 is a plot of $\dot{m}_\Delta/\dot{m}$ vs c/h for $\alpha = 20$ and 90°. Also shown in the figure is a dashed line which depicts how the ratio of the triangular area A_Δ to the total cross sectional area A varies with c/h. The equation of this line is

$$A_\Delta/A = (1 + 2c/h)^{-1}. \tag{18}$$

As expected, the fraction of the mass flow passing through the triangular region decreases as the clearance gap increases. Furthermore, the sharper dropoff of $\dot{m}_\Delta/\dot{m}$ for $\alpha = 20°$, relative to that for 90°, is entirely reasonable.

Of particular interest in Fig. 7 is the comparison of the $\dot{m}_\Delta/\dot{m}$ curves with the curve for the area ratio A_Δ/A. It can be seen that there is a range of c/h, beginning at $c/h = 0$, where $\dot{m}_\Delta/\dot{m} > A_\Delta/A$. Whereas this finding may appear surprising, it can be made physically plausible as follows: for small clearance gaps, the velocities in the entire clearance space are dominated by the retarding action of the lower wall, so that the flow in the space is disproportionately small compared to its area. As the clearance grows larger, the velocities in the clearance space are freed from the wall dominance. Indeed, the general openness of the clearance space, compared with the constraints imposed by the inclined wall of the triangular space, attracts a disproportionately large share of the flow.

PERFORMANCE EVALUATIONS

In evaluating the characteristics of an augmented heat-transfer surface, it is standard practice to compare its performance to a related unaugmented surface. In the present instance, it is natural to compare the corrugated-wall duct to a parallel plate channel. As will be demonstrated shortly, such comparisons will provide perspectives on the role of the parameters α and c/h which characterize the corrugated duct geometry.

In general, performance comparisons are made relative to a specific goal and for prescribed constraints. For example, in a flat plate solar collector, it may be desired to minimize the temperature of the collector plate in order to control extraneous heat losses. To attain this objective, a corrugated-wall duct may be considered in lieu of a parallel plate channel.

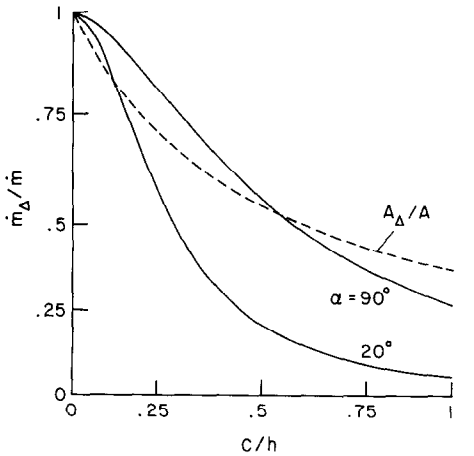

FIG. 7. Cross sectional distribution of mass flow.

The wall temperatures of the two types of ducts may be compared for the condition that the following quantities are the same in the two cases (1) heat input to the fluid per unit axial length; (2) mass flow rate of the fluid; (3) pumping power; (4) spanwise width and (5) streamwise length. A performance analysis directed at the aforementioned goal will now be carried out, subject to the just listed constraints.

To begin, note may be taken of the definition of the pumping power P

$$P = (\dot{m}/\rho)\Delta p. \tag{19}$$

Then, with conditions (2), (3) and (5), it follows that the axial pressure gradient dp/dz is the same for the two types of ducts. Furthermore, since $\bar{u} = \dot{m}/\rho A$, the friction factor equation (13) shows that the value of $(fRe)/AD_e^2$ is the same. If the subscript 0 is used to identify the parallel plate channel and the corrugated duct is unsubscripted, then

$$\frac{A}{A_0}\left(\frac{D_e}{D_{e0}}\right)^2 = \frac{fRe}{(fRe)_0}. \tag{20}$$

If the interplate spacing of the parallel plate channel is H, then $D_{e0} = 2H$, $A/A_0 = (c+\frac{1}{2}h)/H$, and D_e/D_0 follows from equation (2). With these inputs, equation (20) becomes

$$\frac{H}{h} = \left[\frac{4(fRe)_0/fRe}{[1+\mathrm{cosec}(\alpha/2)]^2}\right]^{1/3}\left(\frac{1}{2}+\frac{c}{h}\right). \tag{21}$$

Equation (21) provides the geometrical relationship between the two types of ducts that is consistent with the given constraints. For given values of α and c/h, fRe can be read from Fig. 3; also, $(fRe)_0 = 96$. With these, H/h follows directly from equation (21). The geometrical relationship given by equation (21) will now be employed in the comparative heat-transfer analysis for the two ducts.

For the heat-transfer analysis, attention will be focused on the same heating condition as in the first part of the paper – uniform heat input Q' per unit axial length at the upper surface and adiabatic at the lower surface. If S denotes the surface area of the corrugated wall and S_0 is the surface area of the heated wall of the parallel plate channel, then, with conditions (4) and (5)

$$S/S_0 = \mathrm{cosec}(\alpha/2). \tag{22}$$

Furthermore, since the Q' values are the same for the two cases

$$\bar{q}/\bar{q}_0 = S_0/S. \tag{23}$$

The Nusselt number for the corrugated-wall duct has already been defined in equation (16), and a similar definition applies for the parallel plate channel [the subscript cw (corrugated wall) is replaced by w]. Upon ratioing the Nusselt number definitions and using equations (22) and (23), there is obtained

$$(T_{cw}-T_b)/(T_w-T_b)_0 = (Nu_0/Nu)(D_e/D_{e0})\sin(\alpha/2). \tag{24}$$

Next, it may be noted that $D_e/D_{e0} = D_e/2H$ and that equations (2) and (21) respectively express D_e/h and H/h. When these substitutions are introduced into equation (24), there emerges

$$\frac{T_{cw}-T_b}{(T_w-T_b)_0} = \frac{2(Nu_0/Nu)\sin(\alpha/2)}{[4(1+\mathrm{cosec}(\alpha/2))(fRe)_0/fRe]^{1/3}}. \tag{25}$$

Equation (25) compares the wall-to-bulk temperature rise at the corrugated wall with that at the heated wall of a parallel plate channel. Since conditions (1) and (2) yield equal values of T_b in the numerator and denominator of equation (25), it follows that the ratio $(T_{cw}-T_b)/(T_w-T_b)_0$ provides a direct comparison of the wall temperatures for the two cases. In particular, if the ratio is less than one, then the corrugated-wall duct is successful in fulfilling the original objective of reducing the temperature of the heated wall. The values of Nu and fRe needed to evaluate equation (25) are available from Figs. 4 and 3 for given α and c/h, and $Nu_0 = 5.385$ [1], $(fRe)_0 = 96$.

The temperature ratio expressed by (25) has been plotted as a function of c/h in Fig. 8, with the corrugation angle α as the curve parameter. It is seen from the figure that for the range investigated, the temperature of the corrugated surface is generally lower than that of the heated wall of the parallel plate channel. An interesting feature of the results is that there is a minimum value of the wall temperature for each corrugation angle, with the c/h at the minimum increasing as the angle increases. For $\alpha = 20°$, the minimum occurs near $c/h = 0$, while for $\alpha = 90°$, the minimum is at $c/h \simeq 0.57$. The existence of these minima is an aid to design.

The reductions in wall temperature corresponding to corrugated-wall ducts with small α and small c/h are major. They are, however, bought at the price of substantial increases in heat-transfer surface area. According to equation (22), $S/S_0 = 5.76$ and 2.92 for $\alpha = 20$ and 40°, respectively. Thus, there is a clear first-cost penalty which has to be offset by the greater

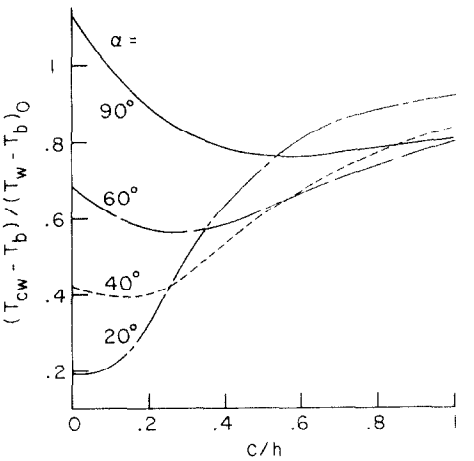

FIG. 8. Wall-to-bulk temperature ratio for corrugated and parallel plate ducts.

operating efficiency afforded by the lower temperature of the wall. The resolution of this economic trade-off is beyond the scope of this paper.

At larger corrugation angles, both the temperature reductions and the area increases are more modest. For $\alpha = 90°$, the minimum value of the temperature ratio is 0.76 while the area ratio $S/S_0 = 1.41$. If the reduction in the temperature ratio were to result in a decrease of the surface temperature of 25–30°F, then an economic analysis would appear to be justified.

It is useful to complement the foregoing presentation of heat-transfer results with information about the geometrical features of the comparison of two types of ducts. In Fig. 9, the cross sectional areas for fluid flow, A and A_0 respectively, are ratioed and plotted as a function of c/h. As expected, the flow cross section for the corrugated duct is generally larger than that for the parallel plate channel, with greater differences in evidence at smaller corrugation angles. For the larger angles, the differences are remarkably small. For example, for $\alpha = 90°$, the maximum value of A/A_0 is about 1.09, and in the range of small c/h it is seen that $A/A_0 < 1$.

Although the cross sectional enlargement of the corrugated duct, relative to the channel, is moderate, the differences between the overall heights may be greater. To examine this matter, the overall height of the corrugated duct $(c + h)$ is ratioed with the height H of the channel and the ratio plotted in Fig. 10. The figure shows that for the parameter range investigated, the height of the corrugated duct exceeds that of the parallel plate channel by at least 50%. For example, for $\alpha = 90°$ and for c/h corresponding to the minimum temperature ratio of Fig. 8, the value of $(c + h)/H$ is 1.58. Thus, if compactness were to be a factor, then there would be some reservations about the use of a corrugated duct.

Up to this point, the performance analysis and evaluation has been aimed at minimizing the surface temperature subject to the constraints listed just before equation (19). Other objectives and other constraints

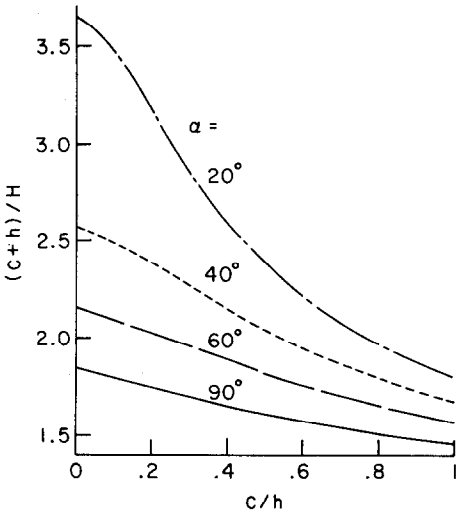

FIG. 10. Duct height ratio for corrugated and parallel plate ducts.

can be considered and, to provide further perspectives, another situation will be briefly examined. Suppose that it is desired to minimize the pumping power P while maintaining the surface temperature the same along with the previously listed quantities (1), (2), (4), and (5). By performing an analysis similar to that described earlier in this section, an expression can be derived for P/P_0 as a function of α and c/h. Numerical evaluation of that expression yields the results shown in Fig. 11. Examination of the figure indicates that appreciable reductions in pumping power can be achieved with the use of a corrugated-wall duct. Especially large decreases are possible when α and c/h are small, but at the price of a large increase of surface area. On the other hand, at a larger angle such as $\alpha = 90°$, the pumping power may be reduced by more than 50% with moderate increases of surface area.

CONCLUDING REMARKS

This paper has described a two-part study of

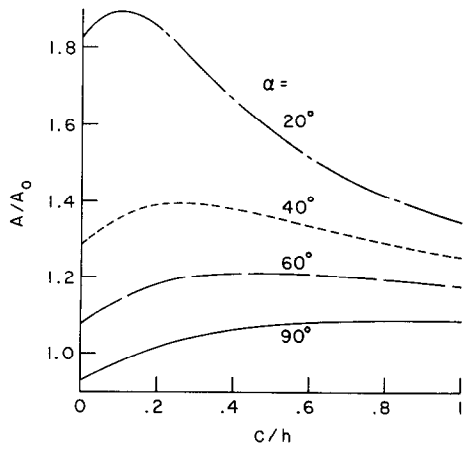

FIG. 9. Cross sectional area ratio for corrugated and parallel plate ducts.

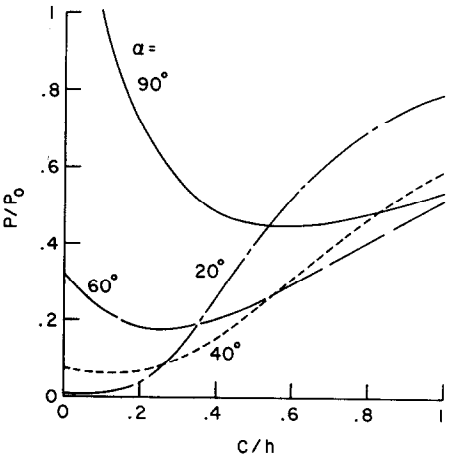

FIG. 11. Pumping power ratio for corrugated and parallel plate ducts.

laminar flow and heat transfer in a spanwise-periodic corrugated duct, encompassing both basic results and performance evaluations. Among the basic results, the friction factor and Nusselt number were presented as a function of the dimension ratio c/h for parametric values of the corrugation angle α. The behaviors of both fRe and Nu were affected by variations of the equivalent diameter D_e as well as by the respective variations of the pressure gradient and the heat-transfer coefficient. Isovel and isotherm maps showed that the cross sectional variations of velocity and temperature become more gradual as the clearance gap increases; the respective peak values also decrease relative to the corresponding averages. Furthermore, with increasing clearance, a greater fraction of the total mass flow passes through the clearance space, but at small clearances the flow through the clearance space is disproportionately small.

The performance evaluations were focused on the comparison of corrugated-wall ducts with the parallel plate channel. Primary attention was given to the minimization of the temperature of the heated wall. It was demonstrated that corrugated ducts can yield substantially lower wall temperatures, but at the price of additional surface area and greater duct height. It was also shown that if pumping power is to be minimized, a corrugated duct can be highly effective, but again with greater surface area and duct height.

Acknowledgement – The research was performed under the auspices of the National Science Foundation (ENG-7518141 A01).

REFERENCES

1. R. K. Shah and A. L. London, *Laminar Flow Forced Convection in Ducts*. Academic Press, New York, 1978.
2. E. Hahne, Personal Communication, Institut für Thermodynamik und Wärmetechnik, University of Stuttgart (June 1978).
3. G. O. G. Lof, Personal Communication, Solaron Corporation, Denver, Colorado, (March 1979).
4. G. S. Beavers, E. M. Sparrow and R. A. Magnuson, Experiments on the breakdown of laminar flow in a parallel plate channel, *Int. J. Heat Mass Transfer* **13**, 809–815 (1970).
5. S. V. Patankar, A numerical method for conduction in composite materials, flow in irregular geometries, and conjugate heat transfer, in *Proceedings, Sixth International Heat Transfer Conference*, Vol. 3, pp. 297–302 (1978).
6. S. V. Patankar, *Numerical Heat Transfer and Fluid Mechanics*. Hemisphere, Washington, D.C. (1980).

CARACTERISTIQUES DU TRANSFERT THERMIQUE ET DE L'ECOULEMENT DANS DES CONDUITES A CORRUGATION PERIODIQUE

Résumé — Il s'agit d'une étude analytique de l'écoulement laminaire et du transfert thermique dans des conduites dont la section droite est limitée par une paroi corrugée de façon périodique tandis que l'autre paroi plane est parallèle à la première. Dans une première partie on étudie l'écoulement et le transfert thermique tandis que dans la seconde partie on utilise et on éclaire les résultats pour évaluer les performances et pour comparer. Les résultats numériques concernent les nombres de Nusselt, les facteurs de frottement, les isovitesses, les isothermes et les distributions de débit massique dans la section droite, avec comparaison avec la conduite à deux parois planes et parallèles. On montre que si la température de la conduite doit être rendue minimale, comme dans les capteurs solaires à air, une conduite corruguée peut être très efficace mais au prix d'un accroissement de surface et d'une plus grande hauteur de conduite.

WÄRMEÜBERGANG UND FLÜSSIGKEITSSTROM IN KANÄLEN MIT PERIODISCH GEWELLTEN WÄNDEN

Zusammenfassung—In einer analytischen Studie wurden Strömung und Wärmeübergang in Kanälen im laminaren Bereich untersucht; der Strömungsquerschnitt ist auf einer Seite von einer Wand begrenzt, die auf der ganzen Breite mit periodischen Wellen versehen ist; die andere begrenzende Wand steht parallel zur gewellten Wand und ist eben. Die Untersuchung besteht aus 2 Teilen, von denen der erste auf die Bereitstellung grundlegender Ergebnisse für den Wärmeübergang und die Strömung abzielt, während im zweiten Teil diese Ergebnisse zur Durchführung von Leistungsberechnungen benutzt und vergleichend erläutert werden. Die grundlegenden Ergebnisse werden numerisch bestimmt und beinhalten Nusselt-Zahlen, Widerstandsbeiwerte, Linien gleicher Geschwindigkeit und Isothermen sowie die Massenstromverteilung über den Querschnitt. Bei den Berechnungen wurden Vergleiche angestellt zwischen einem Kanal mit gewellter Oberfläche und einem Kanal aus parallelen ebenen Platten. Es wird gezeigt, daß dann, wenn die Temperatur der Kanalwand klein gehalten werden soll, wie zum Beispiel bei Luft-Sonnen-kollektoren, ein Kanal mit gewellter Wand sehr wirkungsvoll sein kann; der Preis hierfür ist jedoch zusätzliche Oberfläche und größere Kanalhöhe.

ТЕПЛООБМЕННЫЕ И ГИДРОДИНАМИЧЕСКИЕ ХАРАКТЕРИСТИКИ ГОФРИРОВАННЫХ ПОПЕРЕК ПОТОКА КАНАЛОВ

Аннотация — Проведено аналитическое исследование ламинарного течения и теплопереноса в каналах, одна из стенок которых гофрирована поперек потока, а параллельная ей стенка является гладкой. Работа состоит из двух частей. В первой части представлены основные результаты по теплообмену и гидродинамике, а во второй части даны оценки этих результатов и проведено сравнение с другими данными. В результате численных расчётов получены значения чисел Нуссельта, коэффициентов трения, изотахи и изотермы, а также распределения массового потока по поперечному сечению. Проведено сравнение между каналом с гофрированной стенкой и плоско-параллельным каналом. Показано, что в случае если температура стенок канала должна быть минимизирована, как например, в солнечном коллекторе с воздушным охлаждением, гофрированные каналы являются более эффективными, однако за счёт увеличения площади поверхности и высоты канала.